Generation of an Orbital-Angular-Momentum-Mode-Reconfigurable Beam by a Broadband 1-Bit Electronically Reconfigurable Transmitarray

Baiyang Liu,[†] Sirong Li, Yejun He, Yin Li, and Sai-Wai Wong[*]
College of Electronics and Information Engineering, Shenzhen University, Shenzhen 518061, China

(Received 13 December 2020; revised 3 March 2021; accepted 30 March 2021; published 22 April 2021)

Broadband orbital-angular-momentum (OAM) multiplexing is of great interest due to its ability to increase channel capacity in wireless communications. However, broadband OAM-mode-reconfigurable transmitarrays have yet to be developed. Here, a broadband 1-bit electronically reconfigurable transmitarray for OAM-mode-reconfigurable beam generation is proposed, fabricated, and tested. The OAM transmitarray includes 20×20 elements with a 1-bit phase resolution, each element is controlled by two *p-i-n* diodes with a minimum insertion loss of 0.9 dB and a 3-dB transmission bandwidth of 17.1%. A nearly perfect 1-bit phase resolution is obtained by reversing the current. The OAM mode can be switched between $l = +1$ and $l = +2$ based on a steering-logic board. Both simulation and experiment results show the transmitarray can generate a broadband OAM-mode-reconfigurable beam from 9.5 to 10.5 GHz. The proposed transmitarray may have potential applications in broadband OAM-multiplexing communications.

DOI: 10.1103/PhysRevApplied.15.044035

I. INTRODUCTION

Angular momentum (AM) of electromagnetic (EM) waves can be decomposed into spin angular momentum (SAM) and orbital angular momentum (OAM) [1–3]. OAM-carrying beams can be generated by uniform circular array, metasurfaces, moiré patterns, and grating lenses [4,5]. Recently, OAM has been found in many applications such as particle manipulation, imaging, detecting spinning object, and both quantum and classical communications [1,6–18]. OAM is also expected to resolve the chiral structures due to the chiral phase front. In 2020, using OAM in a microwave plasmonic resonator [19], Cui *et al.* reported the dichrosim of a single particle within the diameter of 1/150 wavelengths and smaller.

One property of vortex waves that has been recently used is the ability to increase channel capacity by multiplexing multiple beams with different modes through a single aperture, such that each vortex beam has a unique rotational phase front. The OAM-multiplexing technology enables different data streams to be transmitted over the same channel. The vortex wave has a rotational phase profile of $\exp(il\theta)$, where θ is the azimuthal angular and l is the unbounded OAM mode [20]. Vortex beams with different OAM modes l are orthogonal to each other, different data streams can be multiplexed together and transmitted along the same beam axis. On the OAM receiver side, the transmitted beams are demultiplexed with low crosstalk, hence the channel capacity and spectral efficiency are increased dramatically. OAM multiplexing has been used in optics, terahertz, millimeter-wave, and microwave communications [13,21,22].

Moreover, researchers have recently used spatiotemporally modulated metasurfaces to generate dynamic OAM beam with special phenomenons. In 2020, Liu *et al.* used dynamic reflective metasurface to observe the electronic rotational Doppler effect [23]. In the same year, Sedeh *et al.* proposed to use time-modulated metasurface to generate optical vortices with self-torque, the OAM mode is varying with both space and time [24].

Recently, broadband OAM generation by antenna array or transmitarray is of great interest due to its ability to achieve high-capacity wireless communications [25–28]. Transmitarray using a planar phase adjusts the surface to produce a prescribed radiation pattern [29–33]. Compared to an OAM-mode-reconfigurable uniform circular array with a complex phase-shifting network when generating high-order OAM mode [34], the programmable transmitarray can achieve OAM-mode reconfigurability by simply changing 1-bit phase distribution. However, the existing broadband OAM transmitarrays are not OAM-mode reconfigurable.

Here we propose a broadband 1-bit electronically reconfigurable OAM transmitarray to generate OAM-mode-reconfigurable beam from 9.5 to 10.5 GHz. The transmitarray consists of one passive patch in receive mode

[*]wongsaiwai@ieee.org
[†]State Key Laboratory of Millimeter Waves, Southeast University, Nanjing, 211189, China.

and one active patch in transmit mode, respectively. The 1-bit phase resolution is obtained by switching two *p-i-n* diodes on the transmit patch thereby reversing its surface current. The element exhibits a minimum insertion loss of 0.9 dB and a 3-dB transmission bandwidth of 17.1% in *X* band. Moreover, the transmitarray based on the designed element is developed to generate OAM-mode-reconfigurable beam by using a steering-logic board. A prototype is validated through far-field and near-field measured results, showing the effectiveness of the proposed transmitarray can generate $l = +1$ and $l = +2$ broadband OAM-mode-reconfigurable beam with high mode purity.

II. THEORETICAL DESIGN

A conceptual representation of the proposed broadband 1-bit electronically reconfigurable OAM transmitarray is shown in Fig. 1. A broadband horn feeder emits an incident wave onto the transmitarray, and the transmitted wave is converted as a broadband OAM-mode-reconfigurable beam. The proposed transmitarray can be spatially modulated by a steering-logic board to realize different OAM phase gradients. The unit cell implemented on the transmitarray is a broadband 1-bit phase-shifting element [35]. It consists of a passive receiving patch on the bottom and an active transmitting patch on the top, which are connected by a metallized via hole located at the center. Both patch antennas are printed on two identical substrate layers, which are Rogers 4003C with a dielectric constant of 3.55 and a loss tangent of 0.0027, and the bonding layer is Rogers 4450F with a dielectric constant of 3.55 and a loss tangent of 0.004. Two *p-i-n* diodes are integrated on the active side to realize a reverse current resulting a 180° phase shifting. MACOM MADP-000907-14020 is chosen as the *p-i-n* diodes in our design. The ground layer is connected to a reference voltage of 2.5 V, and the active layer is connected to a high voltage of 5 V or a low voltage of 0 V, resulting in two different states of *p-i-n*1 *on* *p-i-n*2 *off* and *p-i-n*1 *off* *p-i-n*2 *on*, respectively. Figure 2 shows the explosive view, perspective view, and top view of each layer of the proposed active unit cell, the unit cell is operating in *X* band for *y* polarization.

Simulations of the unit cell are carried out by CST Microwave Studio 2020 using the unit-cell boundary conditions along with Floquet-port excitations. The *p-i-n* diodes are modeled as an equivalent series circuit, resistance $R_{on} = 5.2\ \Omega$ and inductance $L_{on} = 30$ pH while turned *on*, capacitance $C_{off} = 40$ fF and inductance $L_{off} = 30$ pH while turned *off*. As shown in Fig. 3, both operating states exhibit a broadband transmission property but with a 180° phase shifting, which are denoted as 0 state and 180 state, respectively. In order to study the impact of oblique incident and bias lines on the unit-cell frequency response, transmission properties under 40° oblique incident and normal incident with ten bias lines are performed. Figure 3 shows the transmission properties in normal incident, oblique incident at 40°, and normal incident with ten bias lines. In all cases, the minimum insertion loss is 0.9 dB and phase variation is less than 5° from the range of 9.5 to 10.5 GHz. For the case of normal incident without bias lines, the unit cell has a minimum insertion loss of 0.9 dB and 3-dB transmission bandwidth of 17.1%. Moreover, the

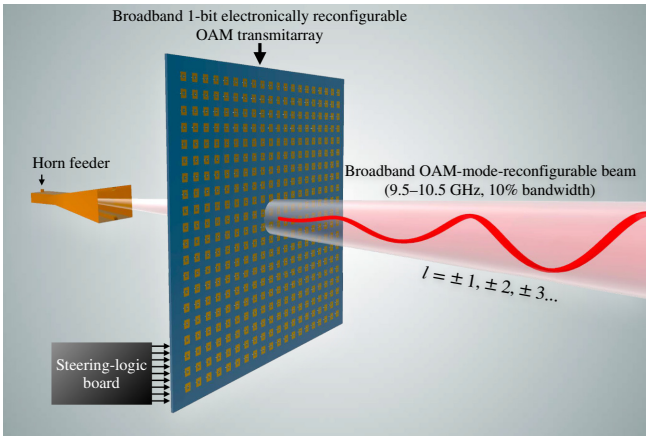

FIG. 1. Conceptual representation of a broadband 1-bit electronically reconfigurable OAM transmitarray, the transmitarray is design at *X* band with a bandwidth of 10%. The transmitted OAM mode can be switched by a steering-logic board.

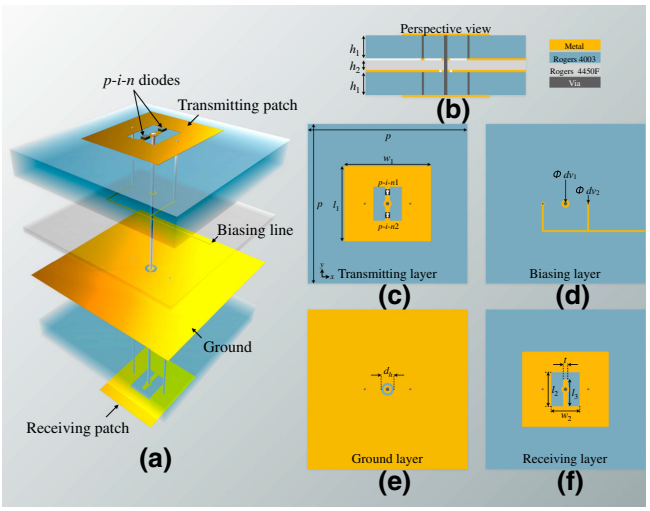

FIG. 2. Design details and parameters of the unit cell for broadband 1-bit electronically reconfigurable OAM transmitarray. (a) Explosive view. (b) Perspective view. (c)–(f) Top view for the transmitting layer, biasing layer, ground layer, and bottom layer, respectively. $h_1 = 1.524$ mm, $h_2 = 0.101$ mm, $p = 14$ mm, $w_1 = 7.7$ mm, $w_2 = 2.5$ mm, $l_1 = 6.7$ mm, $l_2 = 3.1$ mm, $l_3 = 2.3$ mm, $t = 0.4$ mm, $d_h = 1.1$ mm, $d_{v1} = 0.3$ mm, $d_{v2} = 0.15$ mm. The unit cell is designed at the center frequency of 10 GHz with a spacing of 0.466λ.

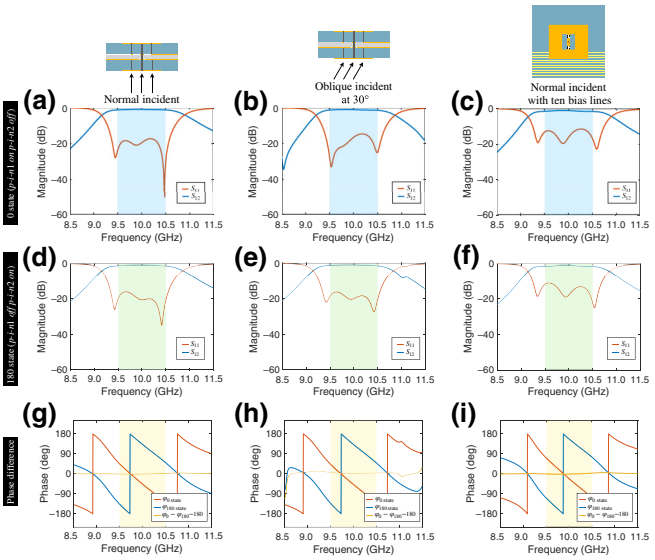

FIG. 3. Simulated magnitude and phase of the transmission coefficient for 0 state and 180 state in different cases. (a)–(c) Unit cell under normal incident. (d)–(f) Unit cell under oblique incident at 40°. (g)–(i) Unit cell under normal incident with ten bias lines; the width of all bias lines is 0.1 mm.

reversing current between two different states exhibits a near-perfect 180° phase shifting in the whole spectrum.

III. BROADBAND 1-BIT ELECTRONICALLY RECONFIGURABLE OAM TRANSMITARRAY

Using the unit cell mentioned above, a transmitarray with $20 \times 20 = 400$ unit cells is developed. Figure 4(a) shows the top view of the broadband 1-bit electronically

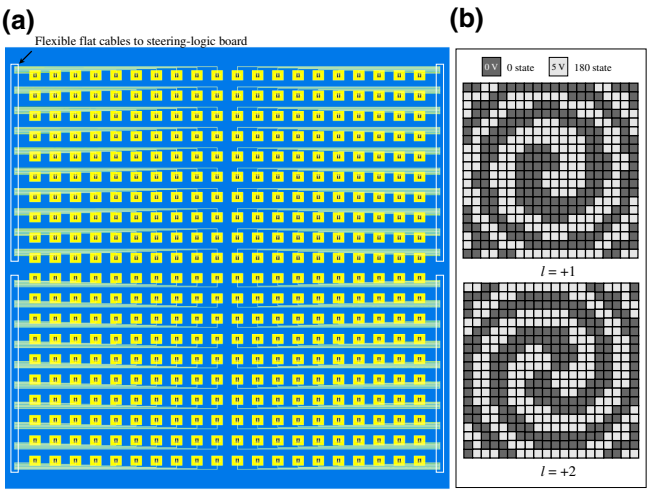

FIG. 4. Layout of a $20 \times 20 = 400$-element broadband 1-bit electronically reconfigurable OAM transmitarray and its biasing network. All the bias lines are connected to a steering-logic board through flexible flat cables. (b) Biasing patterns for $l = +1$ and $l = +2$ OAM beam generation.

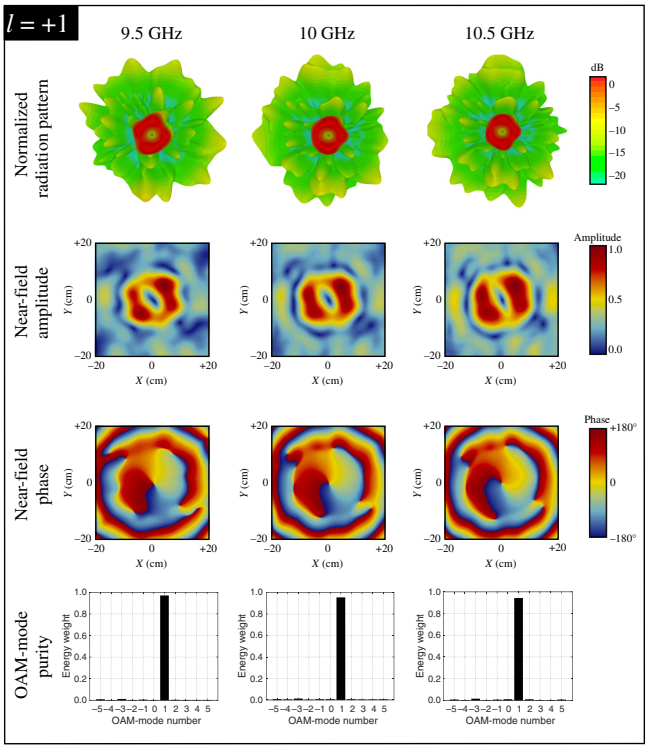

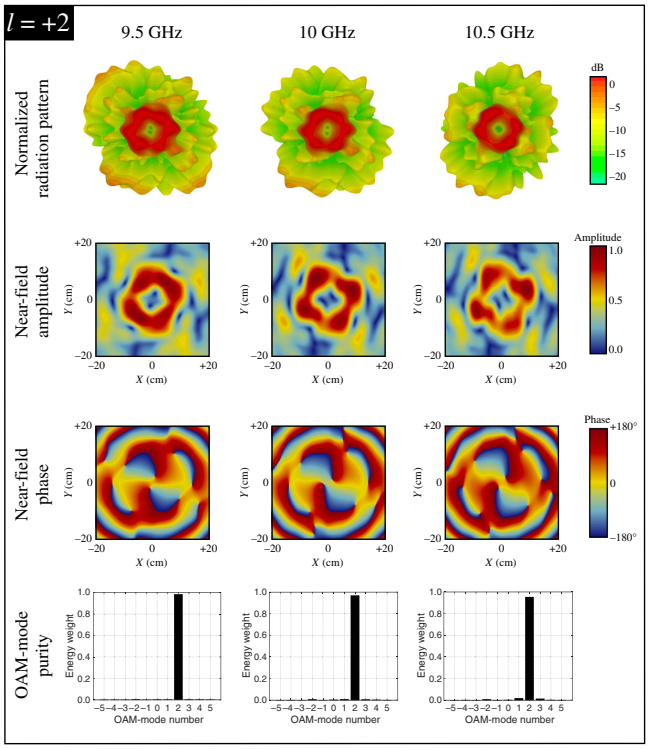

FIG. 5. Simulated results of normalized radiation pattern, near-field amplitude, near-field phase, and OAM mode purity at 9.5, 10.0, and 10.5 GHz for $l = +1$ and $l = +2$.

reconfigurable OAM transmitarray, 400 bias lines are connected to a steering-logic board through flexible flat cables, thereby controlling the transmitted OAM mode. The phase

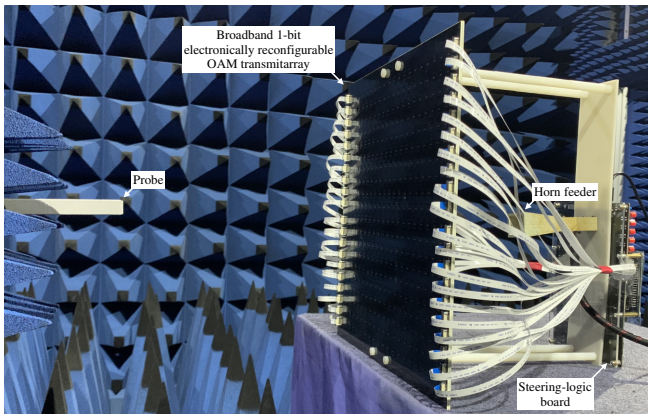

FIG. 6. Overall view of the prototype for broadband OAM-mode-reconfigurable beam generation.

compensation φ of each unit cell to generate a converged OAM beam should satisfy the following condition:

$$\varphi(x,y) = \frac{2\pi\sqrt{x^2+y^2+F^2}-F}{\lambda} + l \times \arctan\left(\frac{x}{y}\right), \tag{1}$$

where l is the OAM mode, x and y are the position of unit cell in Cartesian coordinates, λ is the operating wavelength at a center frequency of 10 GHz, the phase center of the horn feeder is located at the focal point $F = 5\lambda$ of the transmitarray. Moreover, the continuous phase is quantized by a 1-bit phase φ_Q

$$\varphi_Q = \begin{cases} 0, \varphi \in (0+360n, 180+360n] \\ 180, \varphi \in (180+360n, 360+360n] \end{cases}, n \in Z. \tag{2}$$

According to the quantized phase distribution calculated by Eqs. (1) and (2), Fig. 4(b) shows the biasing patterns for $l = +1$ and $l = +2$, respectively. The 0 state is driven by a 5-V high voltage and 180 state is driven by a 0-V low voltage, the ground layer is connected to a reference 2.5-V middle voltage. Note that if we mirror the biasing patterns, $l = -1$ and $l = -2$ OAM beams can also be obtained by the proposed transmitarray.

To characterize an OAM beam, radiation pattern, near-field amplitude, near-field phase, and OAM-mode purity are useful indexes. OAM-mode purity of mode l is constructed as

$$\text{Purity}_l = \frac{|A_l|^2}{\sum_{l=-\infty}^{l=+\infty}|A_l|^2}, \tag{3}$$

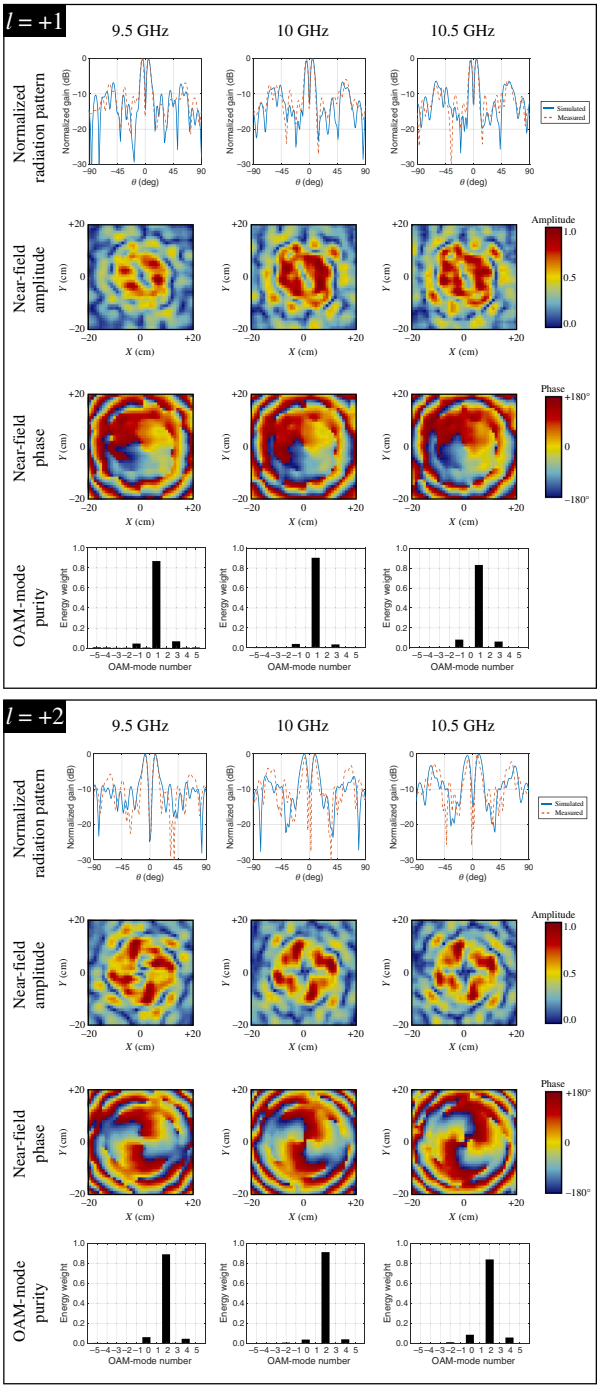

FIG. 7. Measured results of normalized radiation pattern, near-field amplitude, near-field phase, and OAM-mode purity at 9.5, 10.0, and 10.5 GHz for $l = +1$ and $l = +2$.

where A_l is the amplitude of the OAM state, which can be describe as [36]

$$A_l = \frac{1}{2\sqrt{\pi}} \iint_{xy} A(x,y)\exp[j \times \varphi(x,y)] \times \exp\left[-j \times l \times \arctan\left(\frac{x}{y}\right)\right] dxdy. \tag{4}$$

TABLE I. Simulated and measured gain for both OAM modes at different frequencies.

	Frequency		
Mode	9.5 GHz	10.0 GHz	10.5 GHz
Simulated $l = +1$	18.5 dBi	17.3 dBi	16.5 dBi
Measured $l = +1$	17.8 dBi	16.5 dBi	15.7 dBi
Simulated $l = +2$	15.4 dBi	15.1 dBi	14.9 dBi
Measured $l = +2$	14.3 dBi	13.1 dBi	14.2 dBi

The 400-element broadband 1-bit OAM transmitarray is simulated at 9.5, 10.0, and 10.5 GHz, respectively. The simulated normalized radiation pattern, near-field amplitude, near-field phase, and OAM-mode purity for both $l = +1$ and $l = +2$ are shown in Fig. 5. To be specific, the near-field simulated plane is selected at a distance of 5λ away from the transmitarray. From the simulated results we can see the proposed transmitarray can generate a broadband OAM-mode-reconfigurable beam from 9.5 to 10.5 GHz with a mode purity of more than 0.94.

To validate the effectiveness of the proposed broadband 1-bit electronically reconfigurable OAM transmitarray, a prototype is fabricated and tested. The fabricated transmitarray shown in Fig. 6 is coated by a black solder mask, all the *p-i-n* diodes on the transmitarray are soldered by surface-mounting technology. The overall view of the prototype in near-field measurement is illustrated in Fig. 6. Here we measure the performances of the proposed transmitarray in an anechoic chamber, the horn feeder is 5λ away from the transmitarray, and the planar near-field scanner with an open-ended waveguide probe is 5λ away from the transmitarray with an overall scanning range of 40×40 cm^2. The horn feeder is fixed by a polyethylene stand with a dielectric constant of 2.2. Both horn feeder and probe are connected to a network analyzer (Keysight N5224A) to measure the near-field data, the measured results are shown in Fig. 7. Each measured near-field pattern consists of $40 \times 40 = 1600$ electric field data, the scanning resolution is 1 cm in both x and y directions, the scanning time is approximately 30 min for each OAM mode. The measured radiation patterns are also given in Fig. 7, and the simulated and measured gains for both OAM modes at different frequencies are shown in Table I. The measured minimum mode purity over the operating frequency is 0.88, the slight differences between the simulated and measured results are due to the fabrication tolerance, resistance loss of *p-i-n* diodes, and environmental noises. A good agreement is obtained between the simulated and measured results, proving the effectiveness of the proposed broadband 1-bit electronically reconfigurable OAM transmitarray.

IV. CONCLUSION

In summary, we propose a broadband 1-bit electronically reconfigurable OAM transmitarray, the proposed transmitarray can generate an $l = +1$ and $l = +2$ OAM-mode-reconfigurable beam from 9.5 to 10.5 GHz with a measured OAM-mode purity more than 0.88. The measured maximum gains for $l = +1$ and $l = +2$ are 17.8 and 14.3 dBi, respectively. Although our work presents the OAM transmitarray in X band for $l = +1$ and $l = +2$, there is no limitation in using this concept for other frequencies and other OAM modes. This work may provide future directions for broadband programmable transmitarrays and broadband OAM beam generation, and may find potential applications in wireless communications based on OAM multiplexing.

ACKNOWLEDGMENTS

This work is supported in part by the China Postdoctoral Science Foundation under Grant No. 2020M682876, in part by the Guangdong Basic and Applied Basic Research Foundation under Grant No. 2019A1515111127, in part by the State Key Laboratory of the Millimeter Waves Foundation under Grant No. K202113, in part by the Shenzhen Science and Technology Program under Grants No. JCYJ20190808145411289, No. JCYJ20180305124543176, in part by the Natural Science Foundation of Guangdong Province under Grant No. 2018A030313481, and in part by the Shenzhen University Research Startup Project of the New Staff under Grant No. 860-000002110311.

The authors declare no conflicts of interest.

[1] A. M. Yao and M. J. Padgett, Orbital angular momentum: Origins, behavior and applications, Adv. Opt. Photonics **3**, 161 (2011).

[2] R. A. Beth, Mechanical detection and measurement of the angular momentum of light, Phys. Rev. **50**, 115 (1936).

[3] L. Allen, M. W. Beijersbergen, R. J. C. Spreeuw, and J. P. Woerdman, Orbital angular momentum of light and the transformation of Laguerre-Gaussian laser modes, Phys. Rev. A **45**, 8185 (1992).

[4] J. Huguenin, B. C. dos Santos, P. Dos Santos, and A. Khoury, Topological defects in moiré fringes with spiral zone plates, JOSA A **20**, 1883 (2003).

[5] S. Vo, D. Fattal, W. V. Sorin, Z. Peng, T. Tran, M. Fiorentino, and R. G. Beausoleil, Sub-wavelength grating lenses with a twist, IEEE Photonics Technol. Lett. **26**, 1375 (2014).

[6] A. Belmonte and J. P. Torres, Optical Doppler shift with structured light, Opt. Lett. **36**, 4437 (2011).

[7] M. P. Lavery, F. C. Speirits, S. M. Barnett, and M. J. Padgett, Detection of a spinning object using light's orbital angular momentum, Science **341**, 537 (2013).

[8] L. Marrucci, Spinning the Doppler effect, Science **341**, 464 (2013).

[9] M. P. Lavery, S. M. Barnett, F. C. Speirits, and M. J. Padgett, Observation of the rotational Doppler shift of

a white-light, orbital-angular-momentum-carrying beam backscattered from a rotating body, Optica **1**, 1 (2014).
[10] A. Belmonte, C. Rosales-Guzmán, and J. P. Torres, Measurement of flow vorticity with helical beams of light, Optica **2**, 1002 (2015).
[11] G. Li, T. Zentgraf, and S. Zhang, Rotational doppler effect in nonlinear optics, Nat. Phys. **12**, 736 (2016).
[12] S. Franke-Arnold, L. Allen, and M. Padgett, Advances in optical angular momentum, Laser Photonics Rev. **2**, 299 (2008).
[13] J. Wang, J.-Y. Yang, I. M. Fazal, N. Ahmed, Y. Yan, H. Huang, Y. Ren, Y. Yue, S. Dolinar, M. Tur, and *et al.*, Terabit free-space data transmission employing orbital angular momentum multiplexing, Nat. Photonics **6**, 488 (2012).
[14] A. E. Willner, J. Wang, and H. Huang, A different angle on light communications, Science **337**, 655 (2012).
[15] A. E. Willner, H. Huang, Y. Yan, Y. Ren, N. Ahmed, G. Xie, C. Bao, L. Li, Y. Cao, Z. Zhao, *et al.*, Optical communications using orbital angular momentum beams, Adv. Opt. Photonics **7**, 66 (2015).
[16] A. Wang, L. Zhu, S. Chen, C. Du, Q. Mo, and J. Wang, Characterization of LDPC-coded orbital angular momentum modes transmission and multiplexing over a 50-km fiber, Opt. Express **24**, 11716 (2016).
[17] J. Wang, Advances in communications using optical vortices, Photonics Res. **4**, B14 (2016).
[18] Y. Zhao, J. Du, J. Zhang, L. Shen, and J. Wang, Generating structured light with phase helix and intensity helix using reflection-enhanced plasmonic metasurface at 2 μm, Appl. Phys. Lett. **112**, 171103 (2018).
[19] X. Zhang and T. J. Cui, Single-particle dichroism using orbital angular momentum in a microwave plasmonic resonator, ACS Photonics **7**, 3291 (2020).
[20] S. M. Mohammadi, L. K. Daldorff, J. E. Bergman, R. L. Karlsson, B. Thidé, K. Forozesh, T. D. Carozzi, and B. Isham, Orbital angular momentum in radio—A system study, IEEE Trans. Antennas Propag. **58**, 565 (2009).
[21] Y. Yan, G. Xie, M. P. Lavery, H. Huang, N. Ahmed, C. Bao, Y. Ren, Y. Cao, L. Li, Z. Zhao, *et al.*, High-capacity millimetre-wave communications with orbital angular momentum multiplexing, Nat. Commun. **5**, 1 (2014).
[22] B. Liu, 4.8-Gbit/s broadband wireless communication link at radio frequency using orbital angular momentum and polarisation multiplexing, Electron. Lett. **53**, 1248 (2017).
[23] B. Liu, Y. He, S.-W. Wong, and Y. Li, Multifunctional vortex beam generation by a dynamic reflective metasurface, Adv. Opt. Mater. **9**, 2001689 (2020).
[24] H. B. Sedeh, M. M. Salary, and H. Mosallaei, Time-varying optical vortices enabled by time-modulated metasurfaces, Nanophotonics **1**, 55 (2020).
[25] B. Liu, Y. Cui, and R. Li, A broadband dual-polarized dual-oam-mode antenna array for oam communication, IEEE Antennas Wirel. Propag. Lett. **16**, 744 (2016).
[26] J. Wu, Z. Zhang, X. Ren, Z. Huang, and X. Wu, A broadband electronically mode-reconfigurable orbital angular momentum metasurface antenna, IEEE Antennas Wirel. Propag. Lett. **18**, 1482 (2019).
[27] H.-X. Xu, H. Liu, X. Ling, Y. Sun, and F. Yuan, Broadband vortex beam generation using multimode Pancharatnam–Berry metasurface, IEEE Trans. Antennas Propag. **65**, 7378 (2017).
[28] Z. Akram, X. Li, Z. Qi, A. Aziz, L. Yu, H. Zhu, X. Jiang, and X. Li, Broadband high-order OAM reflective metasurface with high mode purity using subwavelength element and circular aperture, IEEE Access **7**, 71963 (2019).
[29] A. Boriskin and R. Sauleau, *Aperture Antennas for Millimeter and Sub-Millimeter Wave Applications* (Springer, Rennes, France, 2018).
[30] D. Pozar, Flat lens antenna concept using aperture coupled microstrip patches, Electron. Lett. **32**, 2109 (1996).
[31] P.-Y. Feng, S.-W. Qu, and S. Yang, Octave bandwidth transmitarrays with a flat gain, IEEE Trans. Antennas Propag. **66**, 5231 (2018).
[32] Q. Luo, S. Gao, M. Sobhy, X. Yang, Z.-Q. Cheng, Y.-L. Geng, and J. T. S. Sumantyo, A hybrid design method for thin-panel transmitarray antennas, IEEE Trans. Antennas Propag. **67**, 6473 (2019).
[33] W. An, S. Xu, F. Yang, and M. Li, A double-layer transmitarray antenna using malta crosses with vias, IEEE Trans. Antennas Propag. **64**, 1120 (2015).
[34] B. Liu, G. Lin, Y. Cui, and R. Li, An orbital angular momentum (OAM) mode reconfigurable antenna for channel capacity improvement and digital data encoding, Sci. Rep. **7**, 1 (2017).
[35] A. Clemente, L. Dussopt, R. Sauleau, P. Potier, and P. Pouliguen, 1-bit reconfigurable unit cell based on pin diodes for transmit-array applications in *x*-band, IEEE Trans. Antennas Propag. **60**, 2260 (2012).
[36] M.-B. Cai, Z.-H. Yan, X.-J. Yi, S.-Y. Yang, and F.-F. Fan, An efficient method of generating vortex electromagnetic wave based on double-layer transmissive metasurface, Int. J. RF Microw. Comput.-Aided Eng. **30**, e22325 (2020).